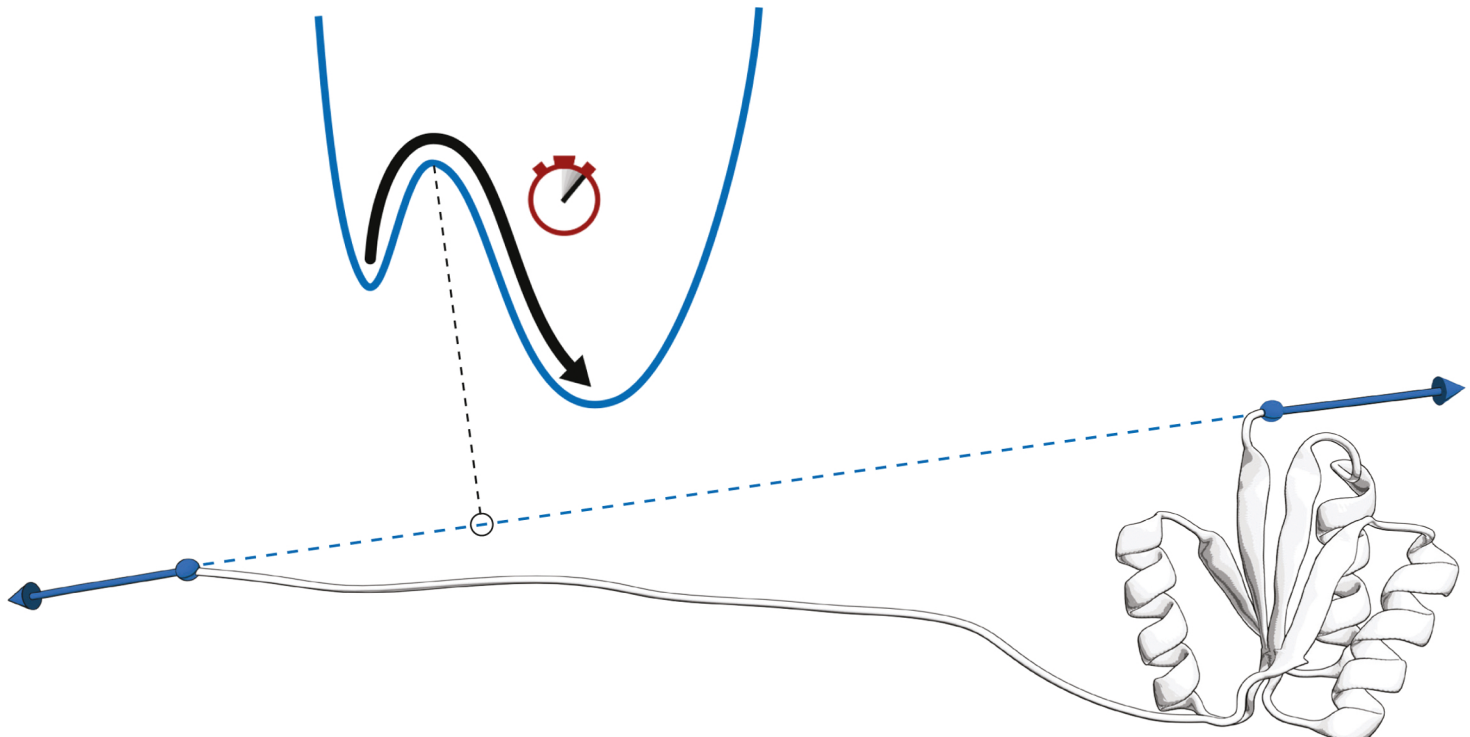


ALEXANDER MEHLICH

TRANSITION PATHS OF PROTEIN-FOLDING
PROBED WITH OPTICAL TWEEZERS

Establishing transition path analysis techniques in single-molecule force spectroscopy based on simulation and experiments performed on natural and artificial proteins

DISSERTATION AT THE PHYSICS DEPARTMENT E22
TECHNISCHE UNIVERSITÄT MÜNCHEN



TECHNISCHE UNIVERSITÄT MÜNCHEN
LEHRSTUHL FÜR BIOPHYSIK E22

**TRANSITION PATHS OF PROTEIN-FOLDING PROBED
WITH OPTICAL TWEEZERS**

Establishing transition path analysis techniques in single-molecule force spectroscopy
based on simulation and experiments performed on natural and artificial proteins

ALEXANDER MEHLICH

Vollständiger Abdruck der von der Fakultät für Physik der Technischen Universität München zur Erlangung
des akademischen Grades eines

Doktors der Naturwissenschaften (Dr. rer. nat.)

genehmigten Dissertation.

Vorsitzender: Prof. Dr. Martin Zacharias

Prüfer der Dissertation: 1. Prof. Dr. Matthias Rief
2. Prof. Dr. Hendrik Dietz

Die Dissertation wurde am 18.10.2017 bei der Technischen Universität München eingereicht und durch die
Fakultät für Physik am 05.12.2017 angenommen.

Alexander Mehlich: *Transition paths of protein-folding probed with optical tweezers*, Establishing transition path analysis techniques in single-molecule force spectroscopy based on simulation and experiments performed on natural and artificial proteins, © October 2017

Berichte aus der Biophysik

Alexander Mehlich

**Transition paths of protein-folding
probed with optical tweezers**

Establishing transition path analysis techniques in single-molecule force spectroscopy based on simulation and experiments performed on natural and artificial proteins

Shaker Verlag
Aachen 2018

Bibliographic information published by the Deutsche Nationalbibliothek

The Deutsche Nationalbibliothek lists this publication in the Deutsche

Nationalbibliografie; detailed bibliographic data are available in the Internet at

<http://dnb.d-nb.de>.

Zugl.: München, Techn. Univ., Diss., 2017

Copyright Shaker Verlag 2018

All rights reserved. No part of this publication may be reproduced, stored in a retrieval system, or transmitted, in any form or by any means, electronic, mechanical, photocopying, recording or otherwise, without the prior permission of the publishers.

Printed in Germany.

ISBN 978-3-8440-5839-0

ISSN 1439-7897

Shaker Verlag GmbH • P.O. BOX 101818 • D-52018 Aachen

Phone: 0049/2407/9596-0 • Telefax: 0049/2407/9596-9

Internet: www.shaker.de • e-mail: info@shaker.de

All that is gold does not glitter,
not all those who wander are lost;
the old that is strong does not wither,
deep roots are not reached by the frost.

— J.R.R. Tolkien

Exponential dependencies are nature's ace in the hole
to make miracles become reality.

— A. M.

ABSTRACT

Proteins are essential for life. To be able to perform their tasks, proteins need to fold into their functional form. From a physicist's perspective, nature solves this 'folding problem' by providing a multidimensional energy landscape which efficiently guides a loose peptide towards a distinct three-dimensional structure which is solely predefined by its unique amino acid sequence. A powerful method to directly study the folding mechanics of proteins is single-molecule force spectroscopy, which is used in this thesis. With a variety of sophisticated analysis tools it is possible to derive transition state positions and barrier heights up to entire one-dimensional projections of the folding energy landscapes of proteins from single-molecule trajectories. Recent technological advances to improve temporal and spatial resolution have opened doors towards directly accessing protein folding transition paths. The establishment of appropriate transition path analysis techniques and their correct interpretation was one of the main objectives of this work.

To this end, transition path analysis techniques were introduced and thoroughly tested using two-dimensional Brownian dynamics simulations. Using this, a very high inter-dependence between the friction involved in protein diffusion and the friction inherent to the detection system was revealed. Owing to this inter-dependence, previously described methods which aim to localise transition states from transition path ensembles or reconstruct barrier heights from committors typically fail to directly provide correct results. Conversely, the strong friction-dependence of detected transition path ensembles have enabled the introduction of a new, merely diffusion-based method of internal protein friction determination. This new method was successfully applied to experimental data of the three-helix bundle protein R15 and revealed the lowest internal friction directly reported from optical tweezers experiments.

The second main objective of this work was the comparison between the folding mechanics of natural and artificial proteins. One artificial protein, a labile re-designed version of the Ferredoxin-like fold, was found to be a relatively simple two-state folder. By contrast, another *de novo* designed protein, the Rossmann fold, was revealed to have an extremely rough energy landscape as opposed to the naturally occurring 'ideal' two-state folder R15. This high energy landscape roughness of the Rossmann fold was characterized by misfolds, multi-pathway folding, a greater effective roughness of $\epsilon_{\text{rms}} = 2.4 \text{ k}_\text{B}T$ with respect to R15, a local roughness of up to $10 \text{ k}_\text{B}T$, two orders of magnitude longer transition path time averages $\langle \tau_{\text{TP}} \rangle$ and, hence, slower folding. Various mutants showed the enforced key lock mechanism of the C-terminal α -helix and its potential bending around position P86 to be the main cause of the folding problems of the Rossmann fold.

The results presented in this work pave the way to a more detailed understanding of protein folding mechanics from a transition path perspective.

ZUSAMMENFASSUNG

Proteine sind lebenswichtig. Um ihre biologischen Aufgaben erfüllen zu können, müssen Proteine ihre funktionsfähige Form durch die sogenannte Faltung annehmen. Aus physikalischer Sicht löst die Natur dieses 'Faltungsproblem' mit Hilfe einer mehrdimensionalen Energienlandschaft, in der ein loses Peptid in seine dreidimensionale Struktur überführt wird, die ausschließlich durch seine einzigartige Aminosäuresequenz vorbestimmt ist. Eine sehr mächtige Methode zur direkten Untersuchung der Faltungsmechanik von Proteinen ist die Einzelmolekül-Kraftspektroskopie, die auch in dieser Arbeit zum Einsatz kommt. Mit einer Vielzahl anspruchsvoller Methoden zur Auswertung von Einzelmolekül-Messungen wurde es möglich, die Position und Energiebarrierenhöhe von Übergangszuständen bis hin zu vollständigen Projektionen eindimensionaler Energienlandschaften der Proteininfaltung zu bestimmen. Die jüngsten technologischen Fortschritte in Bezug auf die zeitliche und räumliche Auflösung haben nun auch die Türen zur direkten Detektion von Übergangspfaden der Proteininfaltung geöffnet. Die Einführung passender Analysemethoden von Übergangspfaden und deren korrekte Interpretation stellen wesentliche Ziele dieser Arbeit dar.

Um dies zu erreichen, wurden Analysemethoden von Übergangspfaden eingeführt und im Rahmen von zweidimensionalen Brownschen Bewegungssimulationen umfassend getestet. Auf diese Art wurde eine starke Abhängigkeit zwischen der Reibung der eigentlichen Proteininfaltung und der Reibung im Messsystem festgestellt. Aufgrund dieser Abhängigkeit scheitern Methoden, die auf der Grundlage von Ensembles aus Übergangspfaden die Position von Übergangszuständen feststellen oder die Höhe von Energiebarrieren rekonstruieren sollen, oft daran, auf direkte Weise korrekte Ergebnisse zu liefern. Im Gegensatz dazu konnte die starke Reibungsabhängigkeit der Ensembles aus Übergangspfaden dazu genutzt werden, eine neue, ausschließlich auf Diffusion basierte Methode zur Bestimmung der inneren Proteinreibung zu entwickeln. Diese neue Methode wurde erfolgreich am dreifachen Helixbündel-Protein R15 angewandt und offenbarte dabei die bisher geringste Reibung, die direkt von Messungen mit optischen Fallen berichtet wurden.

Ein weiteres wichtiges Ziel dieser Arbeit ist es, die Faltungsmechanik von natürlichen und künstlichen Proteinen miteinander zu vergleichen. Ein künstliches Protein, welches ein explizit mechanisch labiles Design des Ferredoxinfaltungsmotivs repräsentiert, wies eine 'einfache' Faltung auf. Ein weiteres *de novo* Protein, das sogenannte Rossmann-Faltungsmotiv, wies hingegen eine extrem raue Energienlandschaft auf, die im völligen Gegensatz zu der 'idealen' Zweizustandsfaltung des natürlichen Proteins R15 steht. Zusammengefasst zeichnet sich die starke Rauheit des Rossmann-Proteins durch eindeutige Hinweise auf Fehlfaltungen, mehrere Faltungspfade, eine gegenüber R15 um $\epsilon_{\text{rms}} = 2.4 \text{ k}_B \text{T}$ erhöhte effektive Reibung, eine lokale Rauheit von bis zu $10 \text{ k}_B \text{T}$ und um zwei Größenordnungen längere mittlere Übergangspfadzeiten $\langle \tau_{\text{TP}} \rangle$

und damit eine entsprechend langsamere Faltung, aus. Verschiedene Mutationen weisen darauf hin, dass der verstärkte Verriegelungsmechanismus der C-terminalen α -Helix und deren Verkrümmung im Bereich der Prolinposition P86 für die Probleme bei der Faltung des Rossmann Proteins verantwortlich sein könnten.

Die Ergebnisse dieser Arbeit ebnen den Weg in Richtung eines besseren Verständnisses der Proteinfaltungsmechanik sowohl im Allgemeinen als auch im Besonderen aus der Sicht von Übergangspfaden.

PUBLICATIONS

While the focus of this thesis lies on unpublished scientific results, a few of the concepts and figures which emerged along with this work can be found in the following publications:

- RINGER P, WEIßL A, COST A.-L., FREIKAMP A, SABASS B, MEHLICH A, TRAMIER M, RIEF M, GRASHOFF C (2017) Multiplexing molecular tension sensors reveals piconewton force gradient across talin-1. *Nature Methods*
- FREIKAMP A, MEHLICH A, KLINGNER C, GRASHOFF C (2016) Investigating piconewton forces in cells by FRET-based molecular force microscopy. *Journal of Structural Biology*
- AUSTEN K¹, RINGER P¹, MEHLICH A¹, CHORSTEK-GRASHOFF A, KLUGER C, KLINGNER C, SABASS B, ZENT R, RIEF M, GRASHOFF C (2015) Extracellular rigidity sensing by talin isoform-specific mechanical linkages. *Nature Cell Biology*
- MEHLICH A¹, AUSTEN K¹, RINGER P¹, RIEF M, GRASHOFF C (2015) Evaluation of molecular tension sensors using single-molecule force spectroscopy and live cell FRET imaging. *Nature Protocol Exchange*²
- FANG J, MEHLICH A, KOGA N, HUANG J, KOGA R, GAO X, HU C, JIN C, RIEF M, KAST J, BAKER D, LI H (2013) Forced protein unfolding leads to highly elastic and tough protein hydrogels. *Nature Communications*
- VON HANSEN Y, MEHLICH A, PELZ B, RIEF M, NETZ R (2012) Auto- and cross-power spectral analysis of dual trap optical tweezer experiments using Bayesian inference. *Review of Scientific Instruments*

¹ These authors contributed equally.

² Non-peer reviewed.

CONTENTS

i	INTRODUCTION	1
1	INTRODUCTION AND MOTIVATION	3
1.1	Solved, or not solved? - the protein-folding problem	3
1.2	The energy landscape perspective	5
1.2.1	Transition paths - distilled essence of reactions	6
1.3	From protein prediction towards protein design	8
1.3.1	Two designed ideal protein structures - Ferredoxin-like fold and Rossmann fold	9
1.4	Thesis outline	10
ii	METHODS, THEORIES, AND DATA ANALYSIS	13
2	EXPERIMENTAL SETUP AND IMPLEMENTATION	15
2.1	How to apply force to a single protein molecule	15
2.1.1	Optical tweezers setup	16
2.1.2	Experimental geometry: the dumbbell assay	17
2.2	Building protein-DNA conjugates	19
2.2.1	Protein-oligonucleotide construct purification	20
2.2.2	Maleimide reactivity test	21
2.2.3	Bioorthogonal chemical coupling alternatives	24
2.3	Experimental modes of force probing	25
2.4	From transitions towards transition paths	28
3	THEORY AND ANALYSIS OF SINGLE MOLECULE EXPERIMENTS	31
3.1	Polymer mechanics	31
3.1.1	Contour length transformation	32
3.2	Free energy calculation	33
3.2.1	Force-dependent probabilities	35
3.3	Fitting equilibrium unfolding/folding transitions	35
3.4	Extracting force-dependent transition rates	36
3.4.1	Rates from force distribution histograms	37
3.4.2	Constructed equilibrium: Oberbarnscheidt's method	37
3.4.3	Rates from lifetime distributions: Hidden Markov model analysis of equilibrium trajectories	38
3.4.4	Pushing limits: autocorrelation analysis	40
3.5	Kinetic models	40
3.5.1	Blind spot at zero force: Arrhenius equation	41
3.5.2	The power of force: Zhurkov-Bell model	41
3.5.3	Force-induced barrier: Schlierf-Berkemeier model	42
3.5.4	Getting in shape: using Kramers theory	44
3.6	Force distribution histograms	46
3.6.1	Elastic compliance: loading rate determination	47
3.7	Deconvolution of probability distributions	49
3.7.1	Setting up the point spread function	50

3.8	Transition Path Analysis	51
3.8.1	Path ensembles and commitment probabilities	52
3.8.2	Committor-based barrier shape reconstruction	54
3.8.3	Bayesian path statistics localise transition states	55
3.8.4	Transition path times and kinetic rates	57
3.8.5	Extracting transition paths	59
iii	SIMULATION RESULTS	63
4	LANGEVIN DYNAMICS SIMULATIONS	65
4.1	Simulation principle	65
4.2	Studies on one-dimensional rough energy landscapes	68
4.2.1	Predicting transition path times and kinetic rates	68
4.2.2	Diffusion in a rough energy landscape	71
4.2.3	Energy landscape reconstruction from transition path times reflecting local roughness	74
4.2.4	A fingerprint for roughness: predominant transition state switching induced by force	79
4.3	Energetically coupled two-dimensional diffusion	81
4.3.1	Deconvolution as a link between dimensions	81
4.3.2	The impact of anisotropic friction on rates, transition path times, and transition path ensembles	84
4.3.3	Transition averages at experimental resolution: seeking traces of protein folding	92
4.3.4	Transition path analysis in force spectroscopy	100
4.4	Summary and Outlook	109
iv	EXPERIMENTAL RESULTS	113
5	FERREDOXIN-LIKE FOLD: MECHANICS OF A TWO-STATE FOLDER	115
5.1	A re-designed ideal protein for tissue engineering	115
5.2	From simple towards complex two-state mechanics	117
5.2.1	Slowing down: approaching equilibrium	117
5.2.2	Varying distance: shifting equilibrium populations	119
5.2.3	How well do different analysis methods agree?	121
5.2.4	Deviations from simple two-state mechanics at low forces	123
5.3	Discussion	125
5.3.1	Force-induced transition state movement: confirming Hammond behaviour by deconvolution	125
5.3.2	Case study FLred: a comparison between the predictive capabilities of different kinetic models	128
5.3.3	Qualitative energy landscape reconstruction	131
5.3.4	Mechanical parameters of designed and natural proteins: revealing a key role of the transition state?	135
5.4	Summary and Outlook	138
5.4.1	Successful protein design verification	138
5.4.2	Application as an <i>in vivo</i> force sensor	139
5.4.3	Force spectroscopy - a test bench for protein design, folding concepts, and models	141

6 ROSSMANN FOLD: AN ARTIFICIAL PROTEIN IN TROUBLE	143
6.1 Design meets evolution: Rossmann vs. R15	143
6.2 A multidimensional and rough energy landscape – a two-state perspective	144
6.2.1 Multiple fingerprints and multi-modal unfolding	144
6.2.2 Split and kinked rate plots	149
6.2.3 Transition averages and prolonged transition path times	152
6.2.4 Deconvolution and commitment probabilities	156
6.2.5 Transition path ensembles and probabilities	161
6.3 Mutants	165
6.3.1 P86A and P86S: proline-free mutants reveal that proline serves as a stabilizing design element	165
6.3.2 S49Cc: directed unfolding of the C-terminal half of ROSS uncovers an energetic imbalance	169
6.3.3 S49Cn and S85Cn: tracing another intermediate	177
6.4 Extended discussion	181
6.4.1 Effective roughness and friction under force	181
6.4.2 Transition-path-assisted protein friction determination	184
6.4.3 Localization and structural interpretation of high-energy intermediates of the Rossmann fold	188
6.4.4 Transition-path-assisted energy landscape reconstruction	192
6.5 Summary and Outlook	195
6.5.1 Folding reliability: evolution outperforms design by means of reduced complexity	196
6.5.2 Transition paths - high potential with imposed limits	202

V APPENDIX 209

A MATERIALS AND METHODS	211
A.1 Protein sequences	211
A.1.1 Ferredoxin-like fold	211
A.1.2 Rossmann fold	212
A.1.3 R15	214
A.1.4 GB1	215
A.1.5 Tension sensors: Ypet-HP35(st)-mCherry	215
A.1.6 Anti-parallel heterodimeric coiled coil: U2LZ	217
A.1.7 Homodimeric coiled coils from kinesin-1	217
A.2 Molecular cloning	217
A.2.1 Functional regions and domains of kinesin-1	217
A.2.2 Design and cloning of coiled coil unzipping constructs	219
A.3 Protocols	224
A.3.1 Protein expression and purification	224
A.3.2 Oligonucleotide attachment details	227
A.3.3 SEC in series with Ni-NTA	234
A.3.4 DNA-handle PCR	238
A.3.5 Sample preparation and measurement at the trap	240

BIBLIOGRAPHY 247

LIST OF FIGURES

Figure 1	Illustration of a protein folding energy landscape.	6
Figure 2	General transition path definition in a simple double-well potential.	7
Figure 3	From protein prediction towards protein design.	8
Figure 4	NMR structures of the Ferredoxin-like fold and the Rossmann fold.	9
Figure 5	Schematic of the optical tweezers setup.	16
Figure 6	Schematic of the dumbbell configuration.	18
Figure 7	SEC purification of an oligonucleotide attachment.	21
Figure 8	Maleimide oligonucleotide reactivity test with DTT.	22
Figure 9	Screening maleimide-thiol reaction parameters.	23
Figure 10	Force-extension trace measured in constant velocity mode.	25
Figure 11	Time traces measured in constant distance mode.	27
Figure 12	Transition paths from highly resolved transitions.	29
Figure 13	Key parameters characterizing folding energy landscapes.	43
Figure 14	Three kinetic models for fitting force-dependent rates.	44
Figure 15	Force distribution histograms and elastic compliance contributions.	48
Figure 16	Illustration of the transition path ensemble and the commitment probability.	53
Figure 17	Commitment probability calculation and committor-based barrier shape reconstruction.	55
Figure 18	Transition path probability calculation and transition state localization.	56
Figure 19	Transition path time averages and distributions.	58
Figure 20	Transition path extraction from simulated and experimental trajectories.	60
Figure 21	2D Langevin dynamics simulation principle.	67
Figure 22	Analysis of transition path times and rates from a 1D diffusion simulation.	69
Figure 23	A thousandfold increase in transition path times induced by energy landscape roughness.	72
Figure 24	Barrier height dependence of dwell times for a given transition state position.	74
Figure 25	Energy landscape reconstruction from transition path times reflecting local roughness.	76
Figure 26	Force induced transition state switching as a fingerprint for roughness.	80
Figure 27	Boltzmann inversion and deconvolution confirm an energetically consistent 2D diffusion simulation.	83
Figure 28	Speed limit protein folding under tension.	85

Figure 29	Friction-dependence of transition path times, rates, and path ensembles of protein folding probed by force.	87
Figure 30	Friction acts as a switch between preferential transition paths.	91
Figure 31	Averaged transitions of the deflection signal with and without inherent protein folding at the 'speed limit'.	94
Figure 32	Averaged transitions of recorded bead dynamics reveal inherent protein folding time scales.	95
Figure 33	Averaged transitions reveal basic features of protein folding energy landscapes.	98
Figure 34	Committor-based barrier reconstruction I: case of a symmetric protein folding energy landscape.	101
Figure 35	Transition path probability calculation I: case of a symmetric protein folding energy landscape.	103
Figure 36	Deconvolution of an asymmetric protein folding energy landscape.	106
Figure 37	Committor-based barrier reconstruction II: case of an asymmetric protein folding energy landscape.	107
Figure 38	Transition path probability calculation II: case of an asymmetric protein folding energy landscape.	108
Figure 39	Positions of the 16 point mutations of FLred.	116
Figure 40	Force-extension traces of FLred at different pulling speeds.	117
Figure 41	Energy landscape parameter reconstruction from data obtained in constant velocity mode.	119
Figure 42	Energy landscape parameter reconstruction from data obtained in constant distance mode.	120
Figure 43	Deviations from simple two-state mechanics at low forces.	124
Figure 44	Transition state movement revealed by deconvolution and energy landscape transformation.	126
Figure 45	The two potential folding units of FLred.	132
Figure 46	Energy landscape reconstruction scenario for FLred.	133
Figure 47	Force sensor performance prediction for FLred.	140
Figure 48	Affecting rates by shifting the transition state position.	141
Figure 49	Crystal and solution NMR structures of the spectrin domain R15 and the 2x2 Rossmann fold.	143
Figure 50	Force spectroscopic fingerprints of ROSS and R15.	145
Figure 51	ROSS has a multi-modal unfolding force distribution.	146
Figure 52	ROSS has split and kinked rate plots.	150
Figure 53	Transition averages of R15 and ROSS.	153
Figure 54	Individual equilibrium transitions and transition path time distributions of R15 and ROSS.	154
Figure 55	Committor-based barrier reconstruction for R15.	157
Figure 56	Committor-based barrier reconstruction for ROSS.	158
Figure 57	R15 and ROSS point towards two fundamental weaknesses of deconvolution.	160
Figure 58	Transition path probability calculation for R15 and ROSS.	162

Figure 59	Proline-free mutants of ROSS by substitution: P86A and P86S. 165
Figure 60	Directed unfolding of the C-terminal half of ROSS: S49Cc. 170
Figure 61	Detailed characterization of the on-pathway intermediate of S49Cc by constant distance measurements. 172
Figure 62	Why β -sheet swapping might cause 'native-like' fingerprints. 175
Figure 63	Directed N-terminal unfolding of ROSS: S49Cn and S85Cn. 178
Figure 64	Effective energy landscape roughness derived from transition path times measured under force. 182
Figure 65	Transition-path-assisted friction coefficient determination of R15. 185
Figure 66	Localization and structural interpretation of high-energy intermediates of ROSS. 189
Figure 67	Transition-path-assisted energy landscape reconstruction for ROSS at 9.5 pN. 193
Figure 68	Reaction schemes for R15 and ROSS. 197
Figure 69	A 'speed limit' reference and candidates for sequence-resolved friction maps. 205
Figure 70	Force-dependent transition path times, histograms, and ensembles. 207
Figure 71	Testing an engineered cysteine crosslink on an SDS-gel. 228
Figure 72	SEC purification of a thiol oligo attachment. 230
Figure 73	Thiol oligo reactivity test with BM(PEG)2. 231
Figure 74	Protein-oligo construct test on an agarose gel. 234
Figure 75	SEC column characterization: resolution and time shifts. 235
Figure 76	Contamination of maleimide oligos revealed by SEC. 236
Figure 77	Improved purification of an oligo attachment reaction by an additional Ni-NTA column. 237

LIST OF TABLES

Table 1	Rate constant calculations: theory versus simulation. 70
Table 2	Detection limit for protein folding transitions. 96
Table 3	Contour gains and folding free energies of FLred from different analysis methods and modes. 121
Table 4	Kinetic parameters of FLred from measurements in constant velocity and constant distance mode. 122
Table 5	Force-induced transition state movement of FLred. 127
Table 6	Energy landscape parameter prediction capabilities of different kinetic models when applied to FLred data. 129
Table 7	Mechanical features of designed and natural proteins. 136

Table 8	Kinetic ZB-model fit parameters of R15 and ROSS based on force distribution histograms. 148
Table 9	Kinetic SB-model fit parameters of R15 and ROSS based on OBS and HMM rates. 151
Table 10	Contour length gains and folding free energies of R15 and ROSS. 152
Table 11	Transition path time averages and bead relaxation times of R15 and ROSS. 155
Table 12	Contour length gains, relative fingerprint occurrences, and folding free energies of ROSS, P86A, and P86S. 166
Table 13	Comparing the kinetics of ROSS and the proline-free mutants P86A and P86S. 167
Table 14	Contour length gains and relative fingerprint occurrences of S49Cc compared to ROSS. 171
Table 15	Comparing the kinetics of S49Cc and ROSS. 171
Table 16	SB-model fit parameters and folding free energies of S49Cc and its obligatory on-pathway intermediate. 173
Table 17	Contour length gains and unfolding characteristics of S49Cc and S85Cc. 179
Table 18	Theoretical speed limit versus experiment: protein friction coefficients implied by transition path times. 183
Table 19	Predominant on-pathway intermediate positions of ROSS. 190
Table 20	Reaction premix for DNA-handle PCR. 239
Table 21	Temperature step protocol for DNA-handle PCR. 239
Table 22	Final measurement mix example. 242

ACRONYMS

AFM Atomic Force Microscope

BM(PEG)2 1,8-Bismaleimido-diethyleneglycol

BSA Bovine Serum Albumin

DTDP 2,2'-Dithiodipyridine

DTT Dithiothreitol

DNA Deoxyribonucleic Acid

FRET Förster Resonance Energy Transfer

FWHM Full Width at Half Maximum

GFP Green Fluorescent Protein

- GODCAT** Glucose/Glucose-Oxidase/Catalase oxygen scavenging system
- HMM** Hidden Markov model
- MD** Molecular dynamics
- NMR** Nuclear Magnetic Resonance
- PBS** Phosphate Buffered Saline
- PCR** Polymerase Chain Reaction
- PSF** Point Spread Function
- RT** Room Temperature
- SEC** Size Exclusion Chromatography
- TCEP** Tris(2-carboxyethyl)phosphine
- TPT** Transition Path Theory
- TST** Transition State Theory
- WHAM** Weighted Histogram Analysis Method
- WLC** Worm-like Chain
- eWLC** extensible Worm-like Chain
- YFP** Yellow Fluorescent Protein